

Relaxed hydrodynamic theory of electrically driven non-equilibrium steady states

Daniel K. Brattan^{1,2,+}, Masataka Matsumoto^{3,4,+}, Matteo Baggioli^{3,4,*}, and Andrea Amoretti^{1,2,*}

¹Dipartimento di Fisica, Università di Genova, via Dodecaneso 33, I-16146, Genova, Italy

²I.N.F.N. - Sezione di Genova, via Dodecaneso 33, I-16146, Genova, Italy

³Wilczek Quantum Center, Shanghai Jiao Tong University, Shanghai 200240, China

⁴Shanghai Research Center for Quantum Sciences, Shanghai 201315, China

*Corresponding authors: b.matteo@sjtu.edu.cn, andrea.amoretti@unige.it

ABSTRACT

Hydrodynamics, as an effective theory capturing long-wavelength and late-time dynamics around thermal equilibrium states, finds applications in diverse physical systems, ranging from electron flow in metals, to ocean wave propagation, traffic flow, bacterial motion and the quark-gluon plasma. On the other hand, non-equilibrium steady states (NESS), characterized by a stationary flow of energy or matter in the presence of a driving force, are pervasive in nature but they present significant challenges to the foundational principles of statistical physics, as it is generally unclear if and how they satisfy the axiomatic assumptions of thermodynamics. The capability of hydrodynamics to accurately describe slow and long-wavelength fluctuations around a NESS remains an open question. In this study, we provide positive evidence by specifically addressing electrically driven non-equilibrium charged steady states. Our approach involves introducing gapped modes and extending the effective description into a relaxed hydrodynamic theory (RHT). Leveraging the gauge-gravity duality as a tool for controlled computations within non-equilibrium systems, we establish an ultraviolet complete model for these NESS that confirms the validity of our RHT. In summary, our findings present a concrete realization of a RHT applicable to a NESS. This expands the regime of validity of hydrodynamics beyond thermal equilibrium, offering valuable insights into the dynamics of non-equilibrium systems.

Introduction

Paraphrasing the timeless wisdom of the Greek philosopher Heraclitus, Marcus Reiner, the pioneer of rheology, once declared, “*Everything flows if you just wait long enough*”. This phrase beautifully captures the essence of hydrodynamics, a framework that extends beyond the realm of fluids to encompass diverse phenomena like electron flow in materials [1], spin wave dynamics in magnets [2], and vibrations in solids [3, 4]. Hydrodynamics, in its broadest sense, offers a theoretical lens for understanding the long-wavelength and late-time dynamics of systems near thermal equilibrium, making it a natural extension of thermodynamics to local equilibrium states.

Non-equilibrium steady states (NESS) emerge when external forces propel a system but that system nevertheless reaches a stationary condition with constant flows of energy, charge, or matter. Unlike undriven global equilibrium states, it is unclear whether NESS have a universal thermodynamic description. Indeed, their nature requires a fundamental rethinking of standard statistical physics assumptions [5–11]. Despite extensive efforts (*e.g.*, [12–15]), it remains uncertain whether hydrodynamics, known for its universality, can adequately describe fluctuations around a NESS.

To illustrate the emergence of NESS and the need for modifying standard hydrodynamics, let us delve into the historical challenge of building a theory of heat conduction. Starting with Fourier law, that links thermal flux $\vec{\mathcal{Q}}$ to temperature gradients by means of the thermal conductivity κ , $\vec{\mathcal{Q}} = -\kappa \vec{\nabla} T$, one immediately encounters the “paradox of heat conduction”. This inconsistency, identified by Nernst [16] and later addressed by Maxwell and Cattaneo [17, 18], highlights the incompatibility of Fourier law with causality. Its resolution necessitates the introduction of a “thermal inertia” parameter τ , marking an early example of what, in modern language, is defined as a quasi-hydrodynamic theory [19, 20], $(1 + \tau \partial_t) \vec{\mathcal{Q}} = -\kappa \vec{\nabla} T$.

In this context, the new parameter τ signifies the time delay required to establish a consistent heat conduction state within a volume element once a temperature gradient is applied. Intriguingly, in the case of most metals, τ is remarkably brief, of the order of picoseconds. This is the rationale for its common omission. Nevertheless, it is worth noting, with a hint of curiosity, that in sand, τ extends to approximately 21 seconds [21]!

Despite its large applicability, the Cattaneo heat equation faced challenges in describing systems in motion, particularly

those in non-equilibrium steady states with a constant background velocity \vec{v}_{drift} [22]. This issue was resolved by Christov and Jordan, who proposed the Cattaneo-Christov model [23–25], restoring Galilean invariance by incorporating a material derivative,

$$\left[1 + \tau \left(\partial_t + \vec{v}_{\text{drift}} \cdot \vec{\nabla} \right)\right] \vec{\mathcal{Q}} = -\kappa \vec{\nabla} T. \quad (1)$$

This modified equation, part of the more general Maxwell-Cattaneo relaxation model [26], finds application in diverse systems, from turbulent flows [27] to chemotaxis [28] and traffic flow [29].

The consequences of the additional terms in equation (1) are striking, since they transform the standard heat diffusion equation into a hyperbolic (and therefore compatible with causality) equation:

$$\tau \frac{\partial^2 T}{\partial t^2} + \frac{\partial T}{\partial t} + \vec{v}_{\text{drift}} \cdot \frac{\partial \vec{\nabla} T}{\partial t} - D \nabla^2 T = \mathcal{R}, \quad (2)$$

with D being the thermal diffusivity and \mathcal{R} some additional driving force.

In recent years, the ability of hydrodynamics to elucidate the intricate flows of electrons and charge conduction in solids [1] has acquired particular significance owing to the engineering of ultra-clean 2D materials, like graphene [30], and the proliferation of strongly coupled materials, exemplified by high temperature superconductors [31], for which a comprehensive microscopic theory remains elusive.

Within solid materials, a steady state can be intuitively achieved through the application of an external electric field. As illustrated by the conventional Drude model [32], conduction electrons subjected to a constant external electric field exhibit a constant drift velocity, wherein the accelerating force is counteracted by the scattering mechanisms that deteriorate the average electronic momentum. The exploration of whether hydrodynamics can effectively capture the fluctuations surrounding this steady state becomes of crucial importance, not only for our comprehension of fundamental conduction properties [33] but also to establish a model of transport in strongly coupled materials where charge is not carried by well-defined quasiparticles [34].

Constructing a robust hydrodynamic theory for a charged fluid under a constant background electric field poses formidable challenges. Early attempts at seamlessly integrating an electric field into hydrodynamic theory presuppose complete compensation by the variation of the chemical potential, resulting in an unphysical equilibrium configuration with a null drift velocity [35].

In a *bona-fide* NESS with non-zero background drift velocity, complexities arise as dissipation effects must necessarily be incorporated into the theory to counterbalance the driving electric field. Notably, both the electric field and the dissipation rates become “thermodynamic variables” within the system, treated on equal footing. Furthermore, the persistence of a constant background drift velocity unavoidably breaks boost invariance, necessitating the application of a boost-agnostic hydrodynamic formalism [36] to achieve a comprehensive understanding [37].

Inspired by recent progress [37], we consider the linearized fluctuations of a relaxed hydrodynamic theory with a conserved $U(1)$ charge density ρ , where the corresponding spatial charge current \vec{J} is weakly non-conserved. This is done in the presence of a background electric field \vec{E} , which is of order zero in derivatives. We demonstrate that the fluctuations of the charge density around the steady state driven by the background electric field must obey a diffusive equation analogous to the Cattaneo-Christov heat equation, (2). The validity of this equation has dramatic consequences on the fluctuations of the charge density which can be put to the test in real materials.

To assess the reliability of our hydrodynamic theory, we compare our predictions against a strongly coupled microscopic UV complete model, the probe brane setup [38], achieved by means of the gauge-gravity duality. These particular models have several key features that make them ideal for exploring (relaxed) hydrodynamics: (I) the onset of the hydrodynamic regime occurs at relatively early times due to the strongly coupled nature of the model, (II) late time tails are consistently truncated out by a large- N expansion meaning all orders in the hydrodynamic derivative expansion can be explored and consequently transport coefficients obtained, and (III) both the collective modes and Green’s functions can be determined by solving relatively simple second order differential equations.

Relaxed hydrodynamic theory

We consider a stationary system in three spatial dimensions with a uniform non-zero charge density ρ and a uniform spatial charge current satisfying $\vec{J} = \sigma_{\text{DC}}(\rho, \vec{E}^2) \vec{E}$, where σ_{DC} is the nonlinear DC charge conductivity. For simplicity, and for consistency with the microscopic model used later, we neglect the fluctuations of energy, temperature and momentum and only consider the dynamics of charge and current fluctuations.

We are interested in fluctuations about this background governed by the charge conservation equation (that follows directly from the $U(1)$ symmetry),

$$\partial_t \delta \rho + \vec{\nabla} \cdot \delta \vec{J} = 0, \quad (3a)$$

where $\delta\rho$ is a linearised fluctuation of the charge density and $\delta\vec{J}$ is a fluctuation of the corresponding spatial charge current. Charge conservation couples to an equation for the evolution of the spatial charge current

$$\partial_t \delta J^i + \partial_j \mathcal{T}^{ij} - \alpha E^i \delta\rho + \frac{1}{\tau} \delta J^i = 0, \quad (3b)$$

where

$$\mathcal{T}^{ij} = v^2 \delta^{ij} \delta\rho + (\eta_1 + \eta_2) \frac{E^i E^j E_k}{\vec{E}^2} \delta J^k + (\eta_2 + \eta_3) E^{(i} \Pi_k^{j)} \delta J^k + (\eta_2 - \eta_3) E^{[i} \Pi_k^{j]} \delta J^k + \eta_4 \Pi^{ij} \delta J^k E_k, \quad (4)$$

and $\Pi^{ij} \equiv \delta^{ij} - \frac{E^i E^j}{\vec{E}^2}$ is a projector with respect to the electric vector field.

This setup generalizes a previous model [39] where the electric field was only considered as a perturbation and the background current vanished (*i.e.*, the background configuration was in global thermal equilibrium and not a NESS). Equations (3a) and (3b) include all terms up to order two in derivatives; in our derivative counting, $\delta\vec{J}$ is order zero in derivatives (similarly to \vec{J}). Also $E^{(i} \Pi_k^{j)}$ and $E^{[i} \Pi_k^{j]}$ indicate respectively the symmetric and antisymmetric parts of the tensor $E^i \Pi_k^j$ with respect to the indices i, j .

By simple manipulations, we find

$$\tau \frac{\partial^2 \delta\rho}{\partial t^2} + \frac{\partial \delta\rho}{\partial t} + \vec{v}_{\text{drift}} \cdot \nabla \delta\rho - D \nabla^2 \delta\rho = \mathcal{R}, \quad (5a)$$

where

$$\vec{v}_{\text{drift}} = -\alpha \tau \vec{E}, \quad D = \tau v^2, \quad (5b)$$

$$\mathcal{R} = \tau \eta_4 \nabla_{\perp}^2 (\vec{E} \cdot \delta\vec{J}) + \tau (\eta_1 + \eta_2) (\vec{E} \cdot \nabla)^2 \vec{E} \cdot \delta\vec{J} + \tau (\eta_2 + \eta_3) (\vec{E} \cdot \nabla) (\nabla_{\perp} \cdot \delta\vec{J}), \quad (5c)$$

and $(\nabla_{\perp})^i = \Pi^{ij} \nabla_j$. If we allow for the fact that the electric field couples directly to the charge density in the drift term, as compared to the temperature which couples through a time derivative, then Eq. (5a) is formally similar to Eq. (2) with \mathcal{R} given in Eq. (5c). The form and need for \mathcal{R} follows from considering all the ways allowed by symmetries that the fluid can couple to the background electric field. Regardless of these technical subtleties, the roles of \vec{v}_{drift} and D for the charge density are physically the same as those for the temperature in Eq. (2).

Now, consider the time (frequency) independent solutions of Eqs. (3a)-(3b). By turning on a time-independent electric field fluctuation, $\delta\vec{E} = i\vec{k} \delta A_t$, with A_t the time component of the external gauge field A_{μ} [40], one finds the retarded charge density correlator

$$\langle \rho \rho \rangle_{\text{R}}(0, \vec{k}) = \frac{|\vec{k}| \chi}{v^2 |\vec{k}| + i \alpha |\vec{E}| \cos \varphi}, \quad (6)$$

where φ is the angle between the wavevector and the electric field and we have ignored terms that are subleading in the $\vec{k}, \vec{E} \rightarrow \vec{0}$ limit.

This result is peculiar from the perspective of standard hydrodynamics. For $\varphi = \pi/2$, in the limit of small wave-vector, we do obtain the standard hydrodynamic result $\chi_{\rho\rho} = \chi/v^2$ [39] with $\chi_{\rho\rho}$ the charge susceptibility in the absence of the electric field. However, for other angles, the charge response is “screened” at small wave-vectors with the effect becoming maximal in the collinear limit $\varphi = 0$. The upshot is that $\langle \rho \rho \rangle_{\text{R}}$ vanishes, rather than attains the charge susceptibility as expected, in the “hydrodynamic limit” of $\vec{k} \rightarrow \vec{0}$ for all angles apart from $\varphi = \pi/2$.

With this stated, we can define the “screening length”

$$\lambda = \frac{D}{|\vec{v}_{\text{drift}}|}, \quad (7)$$

that is formally the inverse of the wave-vector at which the denominator of $\langle \rho \rho \rangle_{\text{R}}(0, \vec{k})$ vanishes. The screening length determines the scale at which the charge response $\langle \rho \rho \rangle_{\text{R}}$ decays to zero and quantifies the relative weight between the diffusive and advective terms in the dynamics of the NESS. In this latter context, it is also customary to define the Peclet number $\text{Pe} \equiv L/\lambda$, that for our system reads

$$\text{Pe} = \frac{L \alpha E |\cos \varphi|}{\tau v^2}, \quad (8)$$

where L is the characteristic length. For $\text{Pe} \gg 1$ diffusion is negligible in the dynamics, while for $\text{Pe} \ll 1$ advection is negligible.

At non-zero frequency (and non-zero wave-vector) the Green's functions can be obtained straightforwardly, see more details in the Supplementary Information (SI). It is worthwhile to note that the DC conductivity is universally related to the spatial charge current susceptibility (χ) and relaxation time (τ) by

$$\sigma_{\text{DC}} = \tau \chi. \quad (9)$$

Moreover, the collective excitations, which quantify how the system disperses perturbations, can be also derived. For \vec{k} parallel to \vec{E} , they are characterized by the following dispersion relations

$$\omega_{\text{gapless}} = \alpha \tau \vec{k} \cdot \vec{E} + \mathcal{O}(\vec{k}^2, \vec{E}^2), \quad (10a)$$

$$\omega_{\text{gapped}} = -\frac{i}{\tau} + (\eta_1 + \eta_2 - \alpha \tau) \vec{k} \cdot \vec{E} + \mathcal{O}(\vec{k}^2, \vec{E}^2), \quad (10b)$$

in the longitudinal sector, while there is a multiplicity two gapped mode with

$$\omega_{\perp} = -\frac{i}{\tau} + \eta_3 \vec{k} \cdot \vec{E} + \mathcal{O}(\vec{k}^2, \vec{E}^2), \quad (10c)$$

in the transverse sector. As is clear from Eqs. (10b)-(10c), the relaxed hydrodynamic theory of such NESS includes gapped degrees of freedom (*i.e.*, modes with $\omega \neq 0$ as $\vec{k} \rightarrow \vec{0}$). Such gapped modes are a consequence of the relaxation mechanisms necessary to maintain the state steady.

A microscopic model of electrically driven NESS

A class of microscopic models that realize electrically driven NESS can be found using the holographic correspondence (or gauge-gravity duality) [41] – a duality between gravitational models and quantum field theories which has been widely exploited for the study of out-of-equilibrium strongly coupled systems [42]. Here, we focus on a holographic probe brane setup [38] in which the backreaction of the charged matter fields on the gravitational background (the thermal bath) is neglected. This setup describes an open system in the regime in which the thermal bath is much larger than the system of interest and consequently dissipation is very efficient. Applying an external electric field to drive the charged particles on the probe brane, one can realize an electrically driven NESS with a stationary current owing to dissipation into the gravitational thermal bath.

Holographically, the degrees of freedom of the thermal bath are described by a black brane in an asymptotically ten-dimensional anti de-Sitter (AdS) spacetime,

$$ds^2 = \frac{\ell^2}{u^2} \left(-f(u) dt^2 + d\vec{x}^2 + \frac{du^2}{f(u)} \right) + \ell^2 d\Omega_5^2, \quad (11)$$

where ℓ is the AdS radius, $f(u) = 1 - u^4/u_H^4$ and $d\Omega_5^2$ is the metric on the 5-sphere. The radial coordinate u ranges from the AdS boundary ($u = 0$) to the black brane horizon ($u = u_H$), and the dual field theory spacetime coordinates are taken as $(t, \vec{x}) = (t, x, y, z)$. The temperature of the thermal bath is given by $T = 1/(\pi u_H)$.

We insert the D7-brane as a probe of the spacetime in Eq. (11), meaning we ignore its backreaction [38]. The dynamics of the U(1) gauge field on the D7-brane is governed by the Dirac–Born–Infeld (DBI) action,

$$S_{D7} = -T_{D7} \int d^8 \xi \sqrt{-\det(g_{ab} + 2\pi\alpha' F_{ab})}, \quad (12)$$

where T_{D7} is the D7-brane tension, ξ^a are the worldvolume coordinates, g_{ab} is the induced metric, and $F_{ab} = \partial_a A_b - \partial_b A_a$ is the field strength of the U(1) gauge field.

For our purposes, we introduce a non-trivial background gauge field: $A_t = A_t(u)$ and $A_x = -Et + h(u)$, where E corresponds to the external electric field along x -direction at the AdS boundary. This background gauge field describes a dual theory [43] with a charge density and current density,

$$\rho = \frac{\mathcal{N} C^2 A'_t}{u \sqrt{1 - C^2 u^4 (A_t'^2 + f^{-1} E^2 - f h'^2)}}, \quad (13a)$$

$$J = \frac{\mathcal{N} C^2 f h'}{u \sqrt{1 - C^2 u^4 (A_t'^2 + f^{-1} E^2 - f h'^2)}}, \quad (13b)$$

where $\mathcal{N} = T_{D7} (2\pi^2) \ell^8 = 2\lambda' N_c / (2\pi)^4$ and $C = 2\pi\alpha' / \ell^2$, in terms of the number of colors N_c , the t'Hooft coupling λ' and the string coupling α' . In this setup, an effective horizon $u_*(T, E)$ emerges outside the black hole horizon as a consequence of

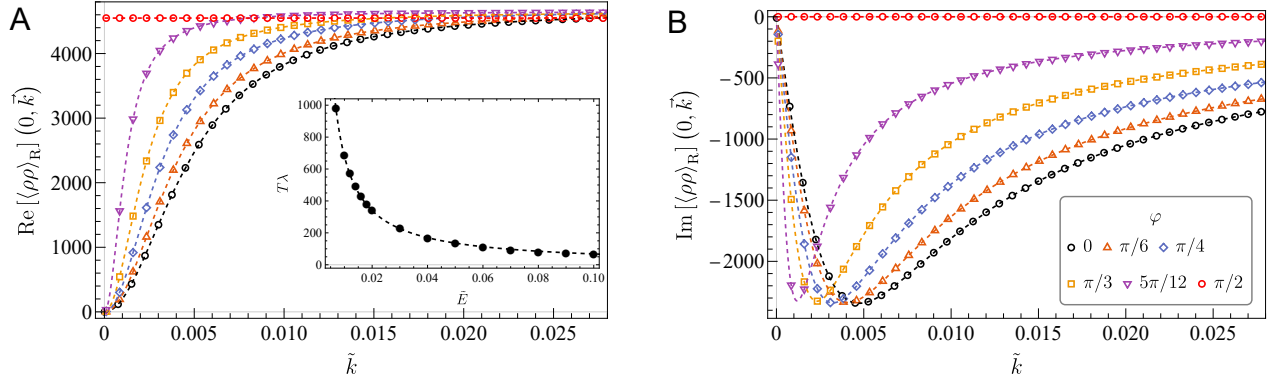


Figure 1. Relaxed hydrodynamic theory vs. microscopic model. Charge-charge static response $\langle \rho \rho \rangle_R(0, \vec{k})$ for different values of the angle φ with $\tilde{\rho} = 10^5$ and $\tilde{E} = 0.1$. (A) The real part and (B) imaginary part are shown. All lines are the predictions of RHT while points are holographic data from the microscopic model. The inset shows the renormalized screening length λ defined in Eq. (7) as a function of the dimensionless electric field \tilde{E} .

the existence of a non-equilibrium state. Evaluating Eqs. (13a)-(13b) at the effective horizon, we can derive the conductivity as a nonlinear function of E in closed form,

$$\frac{\sigma_{\text{DC}}}{\pi T} = \frac{\tilde{J}}{\tilde{E}} = \left(\frac{C^2 \tilde{\rho}^2}{1 + C^2 \tilde{E}^2} + \mathcal{N} C^4 \sqrt{1 + C^2 \tilde{E}^2} \right)^{1/2}, \quad (14)$$

where $(\tilde{J}, \tilde{E}, \tilde{\rho}) \equiv (J/(\pi T)^3, E/(\pi T)^2, \rho/(\pi T)^3)$. In the following analysis, we set $\mathcal{N} = 1$ and $C = 1$ for simplicity.

On top of this non-equilibrium steady state background, we now consider the following fluctuations,

$$A_t \rightarrow A_t(u) + \delta A_t(t, x, y, u), \quad (15a)$$

$$A_x \rightarrow -Et + h(u) + \delta A_x(t, x, y, u), \quad (15b)$$

$$A_y \rightarrow 0 + \delta A_y(t, x, y, u), \quad (15c)$$

where we have chosen to make the fluctuations independent of the z -coordinate owing to the rotational symmetry in the (y, z) -plane. We also use a gauge in which $A_u = 0$ so that the fluctuation of A_z decouples. We then Fourier transform all the fluctuations, $\delta A_\mu(t, \vec{x}, u) = (2\pi)^{-4} \int d\omega d^3k e^{-i\omega t + i\vec{k} \cdot \vec{x}} a_\mu(\omega, \vec{k}, u)$ and we write $\vec{k} \cdot \vec{x} = |\vec{k}|(x \cos \varphi + y \sin \varphi)$, where φ corresponds to the angle between the momentum and background electric field (as in Eq. (6)). Finally, we rescale the frequency and momentum by temperature as $(\tilde{\omega}, \tilde{k}) = (\omega/(\pi T), |\vec{k}|/(\pi T))$.

Subsequently, following the holographic dictionary [44], we impose in-going wave boundary conditions [45], and compute the Green's functions [46]. More details about the computations can be found in the SI.

Pushing hydrodynamics out of equilibrium

We now aim to compare the predictions of the RHT with the numerical simulations performed within the microscopic holographic model. To that end, we start our analysis by considering the fluctuations of the charge density in the static limit encoded in the zero frequency correlator in Eq. (6).

In the large charge density limit $\tilde{\rho} \gg 1$, the values of τ , χ and v^2 are known analytically [39],

$$\frac{1}{\tau} = \frac{(4\pi T)^2}{16c\rho^{1/3}}, \quad \chi_{\rho\rho} = \frac{\rho^{2/3}}{c}, \quad v^2 = \frac{1}{3}, \quad (16)$$

with $c = \Gamma(\frac{1}{3})\Gamma(\frac{1}{6})/(6\sqrt{\pi})$. Thus, in Eq. (6) the only remaining quantity to determine is α . This can be done in two ways: by extracting the complex- \vec{k} position of the pole or, by fitting our hydrodynamic correlator to the holographic data as in Figure 1. Both methods agree to within numerical precision.

In Figure 1 we have chosen a relatively large value of the electric field, $\tilde{E} = 0.1$, to emphasise that our effective description, Eq. (3), applies also in the large electric field limit, on the condition that the charge density is sufficiently big. The reason for

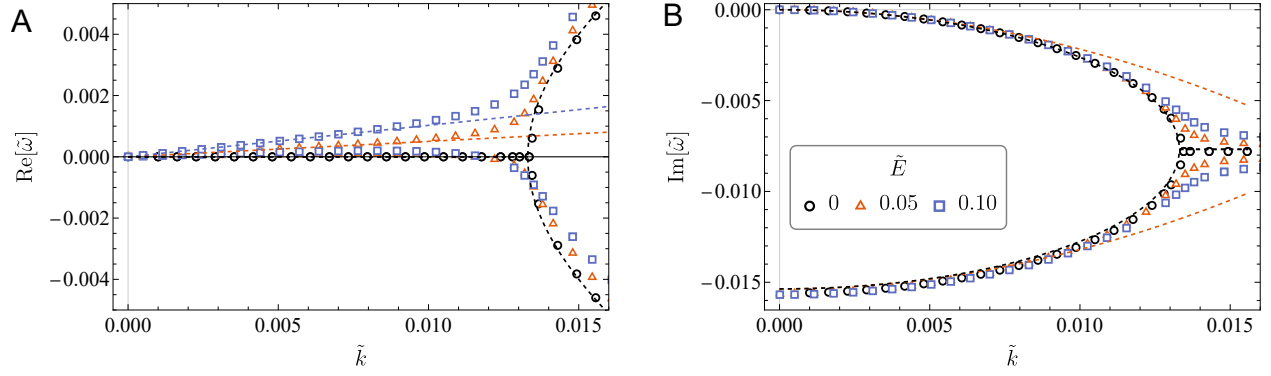


Figure 2. Collective excitations around a non-equilibrium steady state. The dispersion $\tilde{\omega}(\tilde{k})$ of the lowest excitations in the NESS in the collinear limit $\varphi = 0$. (A) The real part and (B) imaginary part of the frequency are shown. Different colors correspond to different strengths of the dimensionless electric field \tilde{E} . The symbols are the data from the microscopic model and the dashed lines are the predictions of RHT.

this is that, as long as ρ is sufficiently large compared to \vec{E} , the gapped modes are very long-lived and the quasi-hydrodynamic (or relaxed approximation) holds.

This suggests that the validity of the relaxed hydrodynamic theory around the NESS does not depend on the strength of the driving nor on the value of the background flow, but it is rather controlled by the relaxation time τ that corresponds to the lifetime of the first non-hydrodynamic mode, or non-conserved quantity.

We remark that the curves in Fig. 1 are not independent fits. On the contrary, we use one curve at a specific angle φ to set α and then all the other curves are parameter-free predictions of the RHT.

The inset of panel (A) in Fig. 1 presents the numerical results for the screening length defined λ in Eq. (7). The prediction of RHT is in good agreement with the numerical data and the screening length decreases monotonically with the value of the electric field. This is a direct manifestation of the fact that increasing the electric field leads to dynamics that are more and more dominated by the drift term rather than thermal diffusive motion.

We then move to consider the dynamical behavior of the system by studying the dispersion relation of the low-energy collective excitations around the NESS. To avoid clutter, we show an explicit comparison only for the longitudinal modes in the collinear limit $\varphi = 0$, but other angles give similar results. The theoretical predictions are presented in Eqs. (10a)-(10b) and involve four parameters: $\tau, \alpha, \eta_1, \eta_2$. In the limit of large charge density, τ is known analytically, Eq. (16), while α is already determined from the static charged correlator mentioned above. Therefore, only η_1 and η_2 are unknown. Unfortunately, because of the structure of the dispersion relation in Eq. (10b), without further information, one can determine only the combination $\eta_{1+2} \equiv \eta_1 + \eta_2$.

As shown in Fig. 2, the theoretical predictions fit the numerical data in the hydrodynamic limit, *i.e.*, $\tilde{k} \ll 1$. Our fits allow us to determine the combination η_{1+2} and yield an interesting relation, $\eta_{1+2} = 4/3\alpha\tau$ that appears robust in the limit considered. We have also compared the theoretical predictions for the transverse excitation, Eq. (10c), and obtained good agreement as well. By following the same procedure and matching the data to the RHT formula Eq. (10c), we find that η_3 , the other unknown parameter appearing in the dispersion relation of the low-energy excitations, is given by $\eta_3 = \alpha\tau$ in the limit of small electric field.

The relations above may be a consequence of some underlying thermodynamic-like identities, however because it is currently not known what the effective free energy is - nor if it exists - we cannot check this. Normally, the free energy would fix certain transport coefficients in terms of derivatives of said free energy, which is also the reason why our model contains more free parameters than would otherwise be expected. For example, we notice that the analysis of the static charge correlator and the low-energy excitations at leading order in \tilde{E} leaves us with two undetermined parameters in the hydrodynamic equation, Eq. (3b). Firstly, we are only able to determine the sum of $\eta_1 + \eta_2$; second, η_4 does not appear in the dispersion of the collective excitations in the limit $\tilde{E} \ll 1$. This would not be the case if the thermodynamics was known.

In order to fully validate the previously derived RHT and all the undetermined “transport coefficients” appearing therein, we need to push the analysis to higher order in the electric field and consider the dynamics at order $\mathcal{O}(\tilde{E}^2)$. In such a limit, Eq. (3b) needs to be generalized to include additional terms that are subleading at order \tilde{E} . The details of this procedure are presented in SI. At order \tilde{E}^2 , the NESS is manifestly anisotropic and all the already discussed quantities split into a parallel contribution and a transverse contribution with respect to the electric field direction. More precisely, both the relaxation time and the velocity split into $\tau_{\parallel}, \tau_{\perp}$ and v_{\parallel}, v_{\perp} .

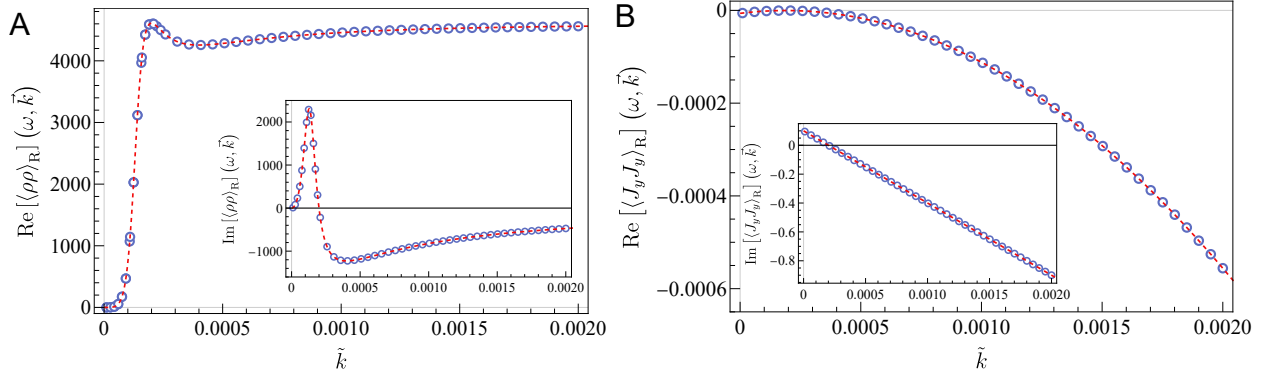


Figure 3. Time dependent dynamics and retarded correlators. The retarded correlators at finite $\tilde{\omega}$ as a function of \tilde{k} in the collinear limit $\varphi = 0$. (A) The charge-charge correlator and (B) perpendicular current-current correlator with $\tilde{\omega} = 10^{-6}$, $\tilde{p} = 10^5$, and $\tilde{E} = 0.005$ are shown. The insets show the imaginary part of the corresponding correlator. The points are the data from the microscopic model and the dashed lines denote the predictions of RHT.

We then consider the complete set of retarded correlators:

$$\langle \rho \rho \rangle_R(\omega, \vec{k}), \quad \langle J^i \rho \rangle_R(\omega, \vec{k}), \quad \langle J^i J^j \rangle_R(\omega, \vec{k}), \quad (17)$$

that can be extracted numerically from the microscopic model and derived theoretically within RHT using the background field method. We emphasize that all these quantities are complex functions and are considered up to $\mathcal{O}(\tilde{E}^2)$. Using the hydrodynamic formulas, we can successfully fit all the correlators and uniquely determine all the transport coefficients appearing in the hydrodynamic theory up to order \tilde{E}^2 .

In Fig.3, we provide an example of a comparison between the hydrodynamic formulas and two of the frequency and wave-vector dependent retarded correlators, $\langle \rho \rho \rangle$ and $\langle J_y J_y \rangle$. The agreement in the hydrodynamic limit is good, confirming the validity of our RHT. In the SI, we show that all the correlators are successfully reproduced by the RHT formulas.

In summary, we have proven the validity of the RHT around a NESS utilising a concrete microscopic model. Importantly, the match between the hydrodynamic theory and the numerical data is not only at the level of the collective excitations but it extends to the whole dynamics in the regime of late times (small frequencies) and large distances (small wave-vectors).

Outlook

We constructed a relaxed hydrodynamic theory describing the late time and long wavelength dynamics of charge and current fluctuations about electrically driven non-equilibrium charge steady states. Our hydrodynamic theory is accompanied by a UV complete model of these NESS, which is built using a holographic probe brane setup within the gauge-gravity duality, and utilized to corroborate our theoretical predictions. The novel hydrodynamic description necessitates the incorporation of relaxation effects – quasi-hydrodynamics – and applies to strongly coupled charged systems as well.

Besides the theoretical extension of hydrodynamics to NESS, our model might have an important impact in the study of charge response in strongly correlated systems or materials without quasiparticles driven by an external electric field [1], for which we provide clear predictions. The charge screening mechanism induced by the NESS drift velocity, and revealed by our analysis, could be in principle verified using locally resolved probe measurements (*e.g.*, scanning single-electron transistors [47] and nitrogen vacancy center magnetometry [48]). At the same time, the time-dependent dynamics could be within reach in pump-probe experiments (*e.g.*, [49]).

Our work provides a significant step towards the applicability of hydrodynamics to non-equilibrium steady states, and it confirms once more its “unreasonable effectiveness”. In the future, it would be interesting to expand our analysis and use the microscopic holographic model to learn more about the thermodynamics of NESS, which remains an important open question in statistical mechanics [11].

References

1. Varnavides, G., Yacoby, A., Felser, C. & Narang, P. Charge transport and hydrodynamics in materials. *Nat. Rev. Mater.* **8**, 726–741, DOI: [10.1038/s41578-023-00597-3](https://doi.org/10.1038/s41578-023-00597-3) (2023).
2. Halperin, B. I. & Hohenberg, P. C. Hydrodynamic theory of spin waves. *Phys. Rev.* **188**, 898–918, DOI: [10.1103/PhysRev.188.898](https://doi.org/10.1103/PhysRev.188.898) (1969).

3. Fleming, P. D. & Cohen, C. Hydrodynamics of solids. *Phys. Rev. B* **13**, 500–516, DOI: [10.1103/PhysRevB.13.500](https://doi.org/10.1103/PhysRevB.13.500) (1976).
4. Martin, P. C., Parodi, O. & Pershan, P. S. Unified hydrodynamic theory for crystals, liquid crystals, and normal fluids. *Phys. Rev. A* **6**, 2401–2420, DOI: [10.1103/PhysRevA.6.2401](https://doi.org/10.1103/PhysRevA.6.2401) (1972).
5. Keizer, J. Thermodynamics at nonequilibrium steady states. *The J. Chem. Phys.* **69**, 2609–2620, DOI: [10.1063/1.436908](https://doi.org/10.1063/1.436908) (2008).
6. Qian, H. Open-system nonequilibrium steady state: Statistical thermodynamics, fluctuations, and chemical oscillations. *The J. Phys. Chem. B* **110**, 15063–15074, DOI: [10.1021/jp061858z](https://doi.org/10.1021/jp061858z) (2006). PMID: 16884217.
7. Lax, M. Fluctuations from the nonequilibrium steady state. *Rev. Mod. Phys.* **32**, 25–64, DOI: [10.1103/RevModPhys.32.25](https://doi.org/10.1103/RevModPhys.32.25) (1960).
8. Zhang, X.-J., Qian, H. & Qian, M. Stochastic theory of nonequilibrium steady states and its applications. part i. *Phys. Reports* **510**, 1–86 (2012). Stochastic Theory of Nonequilibrium Steady States and Its Applications: Part I.
9. Oono, Y. & Paniconi, M. Steady state thermodynamics. *Prog. Theor. Phys. Suppl.* **130**, 29–44 (1998).
10. Sasa, S.-i. & Tasaki, H. Steady state thermodynamics. *J. Stat. Phys.* **125**, 125–224, DOI: [10.1007/s10955-005-9021-7](https://doi.org/10.1007/s10955-005-9021-7) (2006).
11. Lebon, G., Jou, D. & Casas-Vázquez, J. *Understanding non-equilibrium thermodynamics*, vol. 295 (Springer, 2008).
12. Tremblay, A. M. S., Arai, M. & Siggia, E. D. Fluctuations about simple nonequilibrium steady states. *Phys. Rev. A* **23**, 1451–1480, DOI: [10.1103/PhysRevA.23.1451](https://doi.org/10.1103/PhysRevA.23.1451) (1981).
13. Procaccia, I., Ronis, D., Collins, M. A., Ross, J. & Oppenheim, I. Statistical mechanics of stationary states. i. formal theory. *Phys. Rev. A* **19**, 1290–1306, DOI: [10.1103/PhysRevA.19.1290](https://doi.org/10.1103/PhysRevA.19.1290) (1979).
14. Procaccia, I., Ronis, D. & Oppenheim, I. Light scattering from nonequilibrium stationary states: The implication of broken time-reversal symmetry. *Phys. Rev. Lett.* **42**, 287–291, DOI: [10.1103/PhysRevLett.42.287](https://doi.org/10.1103/PhysRevLett.42.287) (1979).
15. Law, B. M. & Sengers, J. V. Fluctuations in fluids out of thermal equilibrium. *J. Stat. Phys.* **57**, 531–547, DOI: [10.1007/BF01022821](https://doi.org/10.1007/BF01022821) (1989).
16. Joseph, D. D. & Preziosi, L. Heat waves. *Rev. Mod. Phys.* **61**, 41–73, DOI: [10.1103/RevModPhys.61.41](https://doi.org/10.1103/RevModPhys.61.41) (1989).
17. Maxwell, J. C. Iv. on the dynamical theory of gases. *Philos. transactions Royal Soc. Lond.* 49–88 (1867).
18. Cattaneo, C. Sur une forme de l'équation de la chaleur éliminant la paradox de propagation instantanée. *Compt. Rendu* **247**, 431–433 (1958).
19. Grozdanov, S., Lucas, A. & Poovuttikul, N. Holography and hydrodynamics with weakly broken symmetries. *Phys. Rev. D* **99**, 086012, DOI: [10.1103/PhysRevD.99.086012](https://doi.org/10.1103/PhysRevD.99.086012) (2019). [1810.10016](https://arxiv.org/abs/1810.10016).
20. Jain, A. & Kovtun, P. Schwinger-Keldysh effective field theory for stable and causal relativistic hydrodynamics. *JHEP* **01**, 162, DOI: [10.1007/JHEP01\(2024\)162](https://doi.org/10.1007/JHEP01(2024)162) (2024). [2309.00511](https://arxiv.org/abs/2309.00511).
21. Chandrasekharaiyah, D. S. Hyperbolic Thermoelasticity: A Review of Recent Literature. *Appl. Mech. Rev.* **51**, 705–729, DOI: [10.1115/1.3098984](https://doi.org/10.1115/1.3098984) (1998).
22. Christov, C. I. & Jordan, P. M. Heat conduction paradox involving second-sound propagation in moving media. *Phys. Rev. Lett.* **94**, 154301, DOI: [10.1103/PhysRevLett.94.154301](https://doi.org/10.1103/PhysRevLett.94.154301) (2005).
23. Christov, C. On frame indifferent formulation of the maxwell–cattaneo model of finite-speed heat conduction. *Mech. Res. Commun.* **36**, 481–486 (2009).
24. Bissell, J. J. On oscillatory convection with the cattaneo–christov hyperbolic heat-flow model. *Proc. Royal Soc. A: Math. Phys. Eng. Sci.* **471**, 20140845, DOI: [10.1098/rspa.2014.0845](https://doi.org/10.1098/rspa.2014.0845) (2015).
25. Straughan, B. Thermal convection with the cattaneo–christov model. *Int. J. Heat Mass Transf.* **53**, 95–98 (2010).
26. Sabelnikov, V. A., Petrova, N. N. & Lipatnikov, A. N. Analytical and numerical study of travelling waves using the maxwell–cattaneo relaxation model extended to reaction–advection–diffusion systems. *Phys. Rev. E* **94**, 042218, DOI: [10.1103/PhysRevE.94.042218](https://doi.org/10.1103/PhysRevE.94.042218) (2016).
27. Bray, K. N. C. & Launder, B. E. Turbulent transport in flames. *Proc. Royal Soc. London. Ser. A: Math. Phys. Sci.* **451**, 231–256, DOI: [10.1098/rspa.1995.0124](https://doi.org/10.1098/rspa.1995.0124) (1995).
28. Berezovskaya, F. S. & Karev, G. P. Bifurcations of travelling waves in population taxis models. *Physics-Uspekhi* **42**, 917, DOI: [10.1070/PU1999v042n09ABEH000564](https://doi.org/10.1070/PU1999v042n09ABEH000564) (1999).

29. Jordan, P. Growth and decay of shock and acceleration waves in a traffic flow model with relaxation. *Phys. D: Nonlinear Phenom.* **207**, 220–229, DOI: <https://doi.org/10.1016/j.physd.2005.06.002> (2005).
30. Lucas, A. & Fong, K. C. Hydrodynamics of electrons in graphene. *J. Physics: Condens. Matter* **30**, 053001, DOI: [10.1088/1361-648x/aaa274](https://doi.org/10.1088/1361-648x/aaa274) (2018).
31. Tranquada, J. M. Cuprate superconductors as viewed through a striped lens. *Adv. Phys.* **69**, 437–509, DOI: [10.1080/00018732.2021.1935698](https://doi.org/10.1080/00018732.2021.1935698) (2020).
32. Chaikin, P. & Lubensky, T. *Principles of Condensed Matter Physics* (Cambridge University Press, 2000).
33. Yu, E. P. *et al.* Use of hydrodynamic theory to estimate electrical current redistribution in metals. *Phys. Plasmas* **27**, 052703, DOI: [10.1063/1.5143271](https://doi.org/10.1063/1.5143271) (2020).
34. Chen, L. *et al.* Shot noise in a strange metal. *Science* **382**, 907–911, DOI: [10.1126/science.abq6100](https://doi.org/10.1126/science.abq6100) (2023).
35. Kovtun, P. Thermodynamics of polarized relativistic matter. *JHEP* **07**, 028, DOI: [10.1007/JHEP07\(2016\)028](https://doi.org/10.1007/JHEP07(2016)028) (2016). [1606.01226](https://arxiv.org/abs/1606.01226).
36. de Boer, J., Hartong, J., Have, E., Obers, N. A. & Sybesma, W. Non-Boost Invariant Fluid Dynamics. *SciPost Phys.* **9**, 018, DOI: [10.21468/SciPostPhys.9.2.018](https://doi.org/10.21468/SciPostPhys.9.2.018) (2020). [2004.10759](https://arxiv.org/abs/2004.10759).
37. Amoretti, A., Brattan, D. K., Martinoia, L. & Matthaiakakis, I. Non-dissipative electrically driven fluids. *JHEP* **05**, 218, DOI: [10.1007/JHEP05\(2023\)218](https://doi.org/10.1007/JHEP05(2023)218) (2023). [2211.05791](https://arxiv.org/abs/2211.05791).
38. Karch, A. & Katz, E. Adding flavor to AdS / CFT. *JHEP* **06**, 043, DOI: [10.1088/1126-6708/2002/06/043](https://doi.org/10.1088/1126-6708/2002/06/043) (2002). [hep-th/0205236](https://arxiv.org/abs/hep-th/0205236).
39. Chen, C.-F. & Lucas, A. Origin of the Drude peak and of zero sound in probe brane holography. *Phys. Lett. B* **774**, 569–574, DOI: [10.1016/j.physletb.2017.10.023](https://doi.org/10.1016/j.physletb.2017.10.023) (2017). [1709.01520](https://arxiv.org/abs/1709.01520).
40. Kovtun, P. Lectures on hydrodynamic fluctuations in relativistic theories. *J. Phys. A* **45**, 473001, DOI: [10.1088/1751-8113/45/47/473001](https://doi.org/10.1088/1751-8113/45/47/473001) (2012). [1205.5040](https://arxiv.org/abs/1205.5040).
41. Ammon, M. & Erdmenger, J. *Gauge/gravity duality: Foundations and applications* (Cambridge University Press, Cambridge, 2015).
42. Liu, H. & Sonner, J. Holographic systems far from equilibrium: a review. *Reports on Prog. Phys.* **83**, 016001, DOI: [10.1088/1361-6633/ab4f91](https://doi.org/10.1088/1361-6633/ab4f91) (2019).
43. Karch, A. & O’Bannon, A. Metallic AdS/CFT. *JHEP* **09**, 024, DOI: [10.1088/1126-6708/2007/09/024](https://doi.org/10.1088/1126-6708/2007/09/024) (2007). [0705.3870](https://arxiv.org/abs/hep-th/0705.3870).
44. Son, D. T. & Starinets, A. O. Minkowski space correlators in AdS / CFT correspondence: Recipe and applications. *JHEP* **09**, 042, DOI: [10.1088/1126-6708/2002/09/042](https://doi.org/10.1088/1126-6708/2002/09/042) (2002). [hep-th/0205051](https://arxiv.org/abs/hep-th/0205051).
45. Mas, J., Shock, J. P. & Tarrío, J. Holographic Spectral Functions in Metallic AdS/CFT. *JHEP* **09**, 032, DOI: [10.1088/1126-6708/2009/09/032](https://doi.org/10.1088/1126-6708/2009/09/032) (2009). [0904.3905](https://arxiv.org/abs/hep-th/0904.3905).
46. Kaminski, M., Landsteiner, K., Mas, J., Shock, J. P. & Tarrío, J. Holographic Operator Mixing and Quasinormal Modes on the Brane. *JHEP* **02**, 021, DOI: [10.1007/JHEP02\(2010\)021](https://doi.org/10.1007/JHEP02(2010)021) (2010). [0911.3610](https://arxiv.org/abs/hep-th/0911.3610).
47. Sulpizio, J. A. *et al.* Visualizing poiseuille flow of hydrodynamic electrons. *Nature* **576**, 75–79, DOI: [10.1038/s41586-019-1788-9](https://doi.org/10.1038/s41586-019-1788-9) (2019).
48. Ku, M. J. H. *et al.* Imaging viscous flow of the dirac fluid in graphene. *Nature* **583**, 537–541, DOI: [10.1038/s41586-020-2507-2](https://doi.org/10.1038/s41586-020-2507-2) (2020).
49. Mitrano, M. *et al.* Ultrafast time-resolved x-ray scattering reveals diffusive charge order dynamics in La₂–xBaCuO₄. *Sci. Adv.* **5**, eaax3346, DOI: [10.1126/sciadv.aax3346](https://doi.org/10.1126/sciadv.aax3346) (2019).
50. Amoretti, A., Brattan, D. K., Martinoia, L. & Matthaiakakis, I. Restoring time-reversal covariance in relaxed hydrodynamics. *Phys. Rev. D* **108**, 056003, DOI: [10.1103/PhysRevD.108.056003](https://doi.org/10.1103/PhysRevD.108.056003) (2023). [2304.01248](https://arxiv.org/abs/2304.01248).
51. Ishigaki, S., Kinoshita, S. & Matsumoto, M. Dynamical stability and filamentary instability in holographic conductors. *JHEP* **04**, 173, DOI: [10.1007/JHEP04\(2022\)173](https://doi.org/10.1007/JHEP04(2022)173) (2022). [2112.11677](https://arxiv.org/abs/2112.11677).

Acknowledgements

M.M. and M.B. acknowledge the support of the Shanghai Municipal Science and Technology Major Project (Grant No.2019SHZDZX01) and the sponsorship from the Yangyang Development Fund. A.A. and D.B. acknowledge support from the project PRIN 2022A8CJP3 by the Italian Ministry of University and Research (MUR). This project has also received funding from the European Union’s Horizon 2020 research and innovation programme under the Marie Skłodowska-Curie grant agreement No. 101030915.

Supplementary information

Green's functions and estimating the transport coefficients

In this Section, we present more details about the formulation of the relaxed hydrodynamic theory and its validation with the microscopic model.

We arrive at our hydrodynamic theory in the main text, valid to $\mathcal{O}(\vec{E}^2)$, by first formulating our effective description without taking the small electric field limit. This is useful for reading off data from the holographic model, as knowing the couplings to background field fluctuations are necessary to accurately extract the various transport coefficients. With this said, the effective equation for the evolution of the charge current takes the form

$$\begin{aligned} \partial_t \delta J^i + \partial_j \left(v_{\parallel}^2 \frac{E^i E^j}{\vec{E}^2} \delta \rho + v_{\perp}^2 \Pi^{ij} \delta \rho + (\eta_1 + \eta_2) \frac{E^i E^j E_k}{\vec{E}^2} \delta J^k + (\eta_2 + \eta_3) E^{(i} \Pi_k^{j)} \delta J^k + (\eta_2 - \eta_3) E^{[i} \Pi_k^{j]} \delta J^k + \eta_4 \Pi^{ij} \delta J^k E_k \right) \\ - \alpha E^i \delta \rho + \frac{1}{\tau_{\parallel}} \frac{E^i E^j}{\vec{E}^2} \delta J_j + \frac{1}{\tau_{\perp}} \Pi^{ij} \delta J_j - \chi_{\parallel} \frac{E^i E^j}{\vec{E}^2} \delta E_j - \chi_{\perp} \Pi^{ij} \delta E_j + \chi_B \Pi^i_j \epsilon^{jkl} E_k \delta B_l + \zeta_{\parallel} \frac{E^i E^j}{\vec{E}^2} \partial_t \delta E_j + \zeta_{\perp} \Pi^{ij} \partial_t \delta E_j \\ + \theta_{\parallel} \frac{E^i E^j}{\vec{E}^2} E^k \partial_k \delta E_j + \theta_{\perp} \Pi^{ij} E^k \partial_k \delta E_j + \theta_{\otimes} E^i \Pi^{jk} \partial_j \delta E_k + \theta_{\bullet} \Pi^{ij} E^k \partial_j \delta E_k + \frac{\theta_B}{\vec{E}^2} \Pi^i_j \epsilon^{jkl} E_k E^m \partial_m \delta B_l + \theta_b E^i \epsilon^{jkl} E_k \Pi_l^m \partial_m \delta B_j \\ + \theta_{\beta} \epsilon^{ijk} E_j \Pi_k^l E^k \partial_l \delta B_k = 0 + \mathcal{O}(\partial^2, \delta^2), \end{aligned} \quad (18)$$

where

$$\delta B_i = \epsilon_i^{jk} \partial_j \delta a_k \quad (19)$$

with a_k a background gauge field and $\Pi^{ij} = \delta^{ij} - \frac{E^i E^j}{\vec{E}^2}$. Imposing the Onsager relations (that are a posteriori validated numerically) upon this expression constrains many of the background field terms but does not constrain the transport coefficients [50] leaving the following quantities undetermined:

$$v_{\parallel}^2, v_{\perp}^2, \alpha, \tau_{\parallel}, \tau_{\perp}, \chi_{\parallel}, \chi_{\perp}, \theta_{\parallel}, \theta_{\perp}, \theta_b, \eta_1, \eta_2, \eta_3, \eta_4. \quad (20a)$$

Consistency in the $\vec{E} \rightarrow \vec{0}$ limit [39] requires that

$$v_{\parallel}^2|_{\vec{E} \rightarrow \vec{0}} = v_{\perp}^2|_{\vec{E} \rightarrow \vec{0}} = v^2, \quad (21a)$$

$$\tau_{\parallel}|_{\vec{E} \rightarrow \vec{0}} = \tau_{\perp}|_{\vec{E} \rightarrow \vec{0}} = \tau, \quad (21b)$$

$$\alpha, \eta_1, \eta_2, \eta_3, \eta_4 \stackrel{\vec{E} \rightarrow 0}{\sim} \mathcal{O}(E^0) \text{ or higher powers.} \quad (21c)$$

Taking the limit of small electric field and turning off the fluctuations of the background field allows us to arrive at the effective theory at small electric field quoted in the main text. Again, when comparing to the holographic model, we must include the couplings to the background gauge field, as these appear as low frequency terms in the holographic correlators, however they disappear in the absence of a background field.

To obtain our transport coefficients from the holographic model, we compute the collective excitations and Green's functions coming from Eq. (18) and linearised charge conservation. To avoid clutter, we will show concrete results for the following choice of parameters, $\vec{E} = 5/1000$ and $\vec{\rho} = 10^5$. Other choices of parameters lead to similar results. We begin considering the collective excitations with \vec{k} parallel to $\vec{E} = (E, 0, 0)$ which allow us to estimate τ_{\parallel} , τ_{\perp} , α , $\eta_1 + \eta_2$ and η_3 ,

$$\omega_{\text{gapless}} = \alpha \tau_{\parallel} \vec{E} \cdot \vec{k} + \mathcal{O}(\vec{k}^2), \quad (22a)$$

$$\omega_{\text{gap}} = -\frac{i}{\tau_{\parallel}} + (\eta_1 + \eta_2 - \alpha \tau_{\parallel}) \vec{E} \cdot \vec{k} + \mathcal{O}(\vec{k}^2), \quad (22b)$$

$$\omega_{\perp} = -\frac{i}{\tau_{\perp}} + \eta_3 \vec{E} \cdot \vec{k} + \mathcal{O}(\vec{k}^2), \quad (22c)$$

in the longitudinal and transverse fluctuation sectors respectively. We find

$$\alpha \tau_{\parallel} \approx \eta_3 \approx 1.000 + \mathcal{O}(\vec{E}^2, \vec{\rho}^{-\frac{1}{3}}), \quad \eta_1 + \eta_2 \approx 1.333 + \mathcal{O}(\vec{E}^2, \vec{\rho}^{-\frac{1}{3}}), \quad (23a)$$

$$\tau_{\parallel}^{-1} \approx (0.713 + 0.358 \vec{E}^2) \vec{\rho}^{-1/3}, \quad \tau_{\perp}^{-1} \approx (0.713 + 0.119 \vec{E}^2) \vec{\rho}^{-1/3}, \quad (23b)$$

where \tilde{E} and $\tilde{\rho}$ are the temperature normalised electric field magnitude and charge density respectively (defined in the main text). Subsequently, using the hydrodynamic relation $\sigma = \tau_{\parallel} \chi_{\parallel} = \tau_{\perp} \chi_{\perp}$, we obtain

$$\chi_{\parallel} = \sigma \tau_{\parallel}^{-1} \approx (0.713 + 0.001 \tilde{E}^2) \tilde{\rho}^{2/3}, \quad (24a)$$

$$\chi_{\perp} = \sigma \tau_{\perp}^{-1} \approx (0.713 - 0.237 \tilde{E}^2) \tilde{\rho}^{2/3}. \quad (24b)$$

In the limit of small electric field, the $\mathcal{O}(\tilde{E}^2)$ corrections to the displayed expressions are below the numerical precision of the leading term and will not be relevant to our initial analysis.

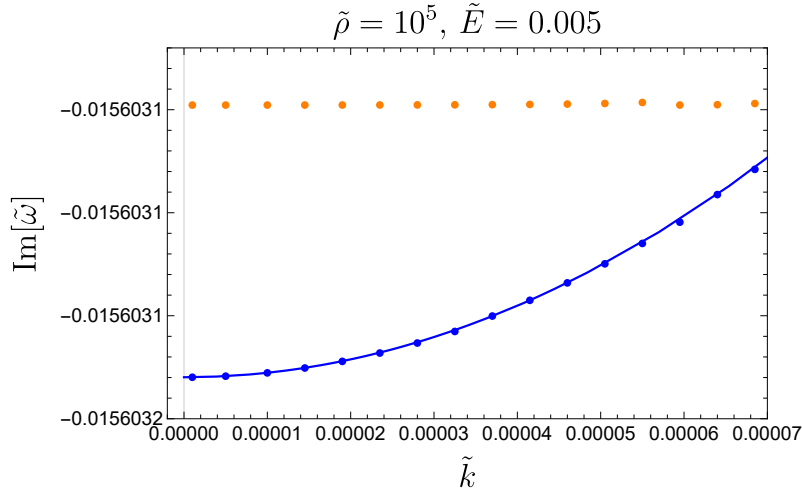


Figure 4. The dispersion relation of two non-hydro modes for small \vec{k} transverse to the electric field with $\tilde{\rho} = 10^5$ and $\tilde{E} = 0.005$. The blue solid line is the prediction from the hydrodynamic theory as explained in the text.

In addition to the above, we can obtain a relation between η_2 and η_4 from the expression for the modes when \vec{k} is transverse to \vec{E} . In particular, choosing the wavevector perpendicular to the electric field breaks the remnant rotational invariance of the system and yields four distinct collective excitations:

$$\omega_{\text{gapless}} = -i \left(v_{\perp}^2 + \alpha \eta_4 \tau_{\parallel} \tilde{E}^2 \right) \vec{k}_{\perp}^2 + \mathcal{O}(\vec{k}_{\perp}^4), \quad (25a)$$

$$\omega_{\text{gap},1} = -\frac{i}{\tau_{\parallel}} + \frac{i \eta_4 \tau_{\parallel} \tau_{\perp} (\alpha \tau_{\parallel} - \eta_2)}{\tau_{\parallel} - \tau_{\perp}} \tilde{E}^2 \vec{k}_{\perp}^2 + \mathcal{O}(\vec{k}_{\perp}^4), \quad (25b)$$

$$\omega_{\text{gap},2} = -\frac{i}{\tau_{\perp}} + i \left(\left(v_{\perp}^2 + \alpha \eta_4 \tau_{\parallel} \tilde{E}^2 \right) - \frac{\eta_4 \tau_{\parallel} \tau_{\perp} (\alpha \tau_{\parallel} - \eta_2)}{\tau_{\parallel} - \tau_{\perp}} \tilde{E}^2 \right) \vec{k}_{\perp}^2 + \mathcal{O}(\vec{k}_{\perp}^4), \quad (25c)$$

$$\omega_{\text{gap},3} = -\frac{i}{\tau_{\perp}} + \mathcal{O}(\vec{k}_{\perp}^4). \quad (25d)$$

The imaginary part of one of the gapped modes, displayed in figure 4 with orange color, is independent of \vec{k} for small \vec{k} in the range of \tilde{E} and $\tilde{\rho}$ considered. Using this and our previously obtained values for the transport coefficients, Eqs. (23)-(24), we find the following relation

$$(1 - \eta_2) \eta_4 = -0.112. \quad (26)$$

Substituting this relation into the expression for the second gapless mode, displayed as the solid blue line in figure 4, we find consistency. We have checked this result for various large values of $\tilde{\rho}$ and small \tilde{E} and obtained the same positive result.

To extract the remaining transport coefficients we compare holographic data against our Green's functions. We obtain the Green's functions through the background field method where one turns on a perturbation of the background gauge field which

acts as a force in the equations of motion. The retarded correlators are then given by

$$\langle \rho \rho \rangle_{\text{R}}(\omega, \vec{k}) = \lim_{\delta A \rightarrow 0} \frac{\delta \langle \rho \rangle_{\delta A}}{\delta A_t}, \quad (27a)$$

$$\langle J^i \rho \rangle_{\text{R}}(\omega, \vec{k}) = \lim_{\delta A \rightarrow 0} \frac{\delta \langle J^i \rangle_{\delta A}}{\delta A_t}, \quad (27b)$$

$$\langle \rho J^j \rangle_{\text{R}}(\omega, \vec{k}) = \lim_{\delta A \rightarrow 0} \frac{\delta \langle \rho \rangle_{\delta A}}{\delta A_j}, \quad (27c)$$

$$\langle J^i J^j \rangle_{\text{R}}(\omega, \vec{k}) = \lim_{\delta A \rightarrow 0} \frac{\delta \langle J^i \rangle_{\delta A}}{\delta A_j}, \quad (27d)$$

where $\delta \langle \rho \rangle_{\delta A}$ and $\delta \langle J^i \rangle_{\delta A}$ indicate the fluctuations of the one-point functions in the presence of the linearised perturbation of the gauge field. In practice, for our situation, this amounts to nothing more than solving for the Fourier modes of Eq. (18) plus charge conservation with the fluctuation of the gauge fields acting as a source.

The parameters v_{\parallel}^2 and θ_{\parallel}

At zero frequency, the retarded correlator of the charge density for \vec{k} parallel to \vec{E} takes the form

$$\langle \rho \rho \rangle(0, \vec{k}) = \frac{|\vec{k}|(\chi_{\parallel} + |\vec{E}||\vec{k}|\theta_{\parallel})}{v_{\parallel}^2|\vec{k}| + i\alpha|\vec{E}|}. \quad (28)$$

We fit the real part of this function, which turns out to be the most sensitive to the value of θ_{\parallel} , to the numerical data and extract v_{\parallel}^2 and θ_{\parallel} . The subsequent fit is displayed in Fig. 5a. To produce Fig. 5b we introduce a large \vec{k} cut-off and then extract v_{\parallel}^2 and θ_{\parallel} only for data with $|\vec{k}| < k_{\text{cutoff}}$. Plotting the change in the transport coefficients as the cut-off is reduced illustrates the stability in their values.

The parameter θ_{β}

The θ_{β} transport coefficient is readily extracted from $\langle J^z J^z \rangle(0, \vec{k})$ with k perpendicular to \vec{E} as

$$\langle J^z J^z \rangle(0, \vec{k}) = -\theta_{\beta} \tau_{\perp} \vec{E}^2 \vec{k}^2 + \mathcal{O}(\vec{k}^3). \quad (29)$$

We find (for $\vec{E} = 5/1000$) that

$$\theta_{\beta} \approx 5.75 \times 10^3. \quad (30)$$

The parameter v_{\perp}^2

At the value of \vec{E} we are examining, in the stated range of \vec{k} , the correlator $\langle J_y J_y \rangle$ at zero frequency with \vec{k} parallel to \vec{E} is approximately quadratic in the real part and linear in the imaginary part. The numerical correlator is approximately

$$\langle J_y J_y \rangle(0, \vec{k}) \approx -499.987 i \vec{k} - 169.411 \vec{k}^2 + \mathcal{O}(\vec{k}^3), \quad (31)$$

which is displayed in Figs. 5c and 5d.

In our hydrodynamic expressions, the linear piece is already fixed by the coefficients we have already determined and we find $\text{Im}[\langle J_y J_y \rangle] \sim -499.994$ which represents a good agreement. The real part of the correlator can be used to fix an expression for v_{\perp}^2 in terms of η_1 and θ_b , namely

$$v_{\perp}^2 \approx 0.338 + 2.500 \times 10^{-5} \eta_1 + 2.500 \times 10^{-10} \theta_b. \quad (32)$$

Consequently, we expect the leading term to dominate v_{\perp}^2 for reasonable values of η_1 and θ_b . This will be confirmed shortly.

The parameters θ_b and η_1

The leading term in small k for $\langle J_t J_t \rangle(0, \vec{k})$ with \vec{k} perpendicular to \vec{E} is

$$\langle J_t J_t \rangle(0, \vec{k}) = \frac{\chi_{\perp}}{v_{\perp}^2 + \alpha \vec{E}^2 \eta_4 \tau_{\parallel}} + \mathcal{O}(\vec{E}^4 \vec{k}^2). \quad (33)$$

We expect the subleading term to be strongly affected by precision errors, which bears out if we use it to fix some of our remaining transport coefficients and compare against other correlators. From Eq. (33) we can determine an expression for θ_b in

terms of η_1 . Subsequently, we minimise the least square difference between our expression for the finite frequency correlator $\langle J_y J_y \rangle (10^{-6}, \vec{k})$ with \vec{k} parallel to \vec{E} for η_1 as this seems to be the most sensitive to these values. We find

$$\eta_1 \approx 1.27, \quad \theta_b \approx -7.99 \times 10^4. \quad (34)$$

The stability of these transport coefficients is shown in Fig. 5e where we plot them against varying the cut-off wave-vector.

Summary

The values for the transport coefficients and background field couplings with $\tilde{E} = 5/1000$ are approximately

$$\tau_{\parallel}, \tau_{\perp} \approx 64.1, \quad \alpha \approx 0.0156, \quad v_{\parallel}^2, v_{\perp}^2 \approx 0.338, \quad \chi_{\parallel}, \chi_{\perp} \approx 1.56 \times 10^3, \quad \theta_{\parallel} \approx -1.66 \times 10^4, \quad \theta_b \approx -7.99 \times 10^4, \quad (35a)$$

$$\theta_{\beta} \approx 5.75 \times 10^3, \quad \eta_1 \approx 1.27, \quad \eta_2 \approx 0.0485, \quad \eta_3 \approx 1.000, \quad \eta_4 \approx -0.117. \quad (35b)$$

A more detailed technical analysis is necessary to fix our transport coefficients precisely. We summarise our fits in Fig. 6 for the zero frequency correlators and Fig. 7 for the non-zero frequency ($\omega = 10^{-6}$) correlators.

Linear perturbations in the holographic probe brane model

In this Section, we present more details about the microscopic holographic model.

In the main text, we consider the following gauge field fluctuations on the steady state background,

$$A_t \rightarrow A_t(u) + \delta A_t(t, x, y, u), \quad (36a)$$

$$A_x \rightarrow -Et + h(u) + \delta A_x(t, x, y, u), \quad (36b)$$

$$A_y \rightarrow 0 + \delta A_y(t, x, y, u). \quad (36c)$$

Choosing the gauge $A_u = 0$, we obtain the constraint for the other fluctuations $\{\delta A_t, \delta A_x, \delta A_y\}$:

$$\begin{aligned} -\frac{1}{R} \left[-g^{tt} g^{uu} (1 + g^{tt} g^{xx} E^2 + g^{xx} g^{uu} h'^2) (\partial_t \delta A_t') - g^{xx} g^{uu} (1 + g^{tt} g^{xx} E^2 + g^{tt} g^{uu} A_t'^2) (\partial_x \delta A_x') \right. \\ \left. + g^{tt} g^{xx} (g^{uu})^2 A_t' h' (\partial_x \delta A_t' + \partial_t \delta h') - g^{tt} (g^{xx})^2 g^{uu} E h' (\partial_x f_{tx}) - (g^{tt})^2 g^{xx} g^{uu} E A_t' (\partial_t f_{tx}) \right] \\ + g^{tt} g^{xx} g^{yy} g^{uu} E h' (\partial_y f_{ty}) - g^{tt} g^{xx} g^{yy} g^{uu} E A_t' (\partial_y f_{xy}) + g^{yy} g^{uu} (1 + g^{tt} g^{xx} E^2) (\partial_y \delta A_y') = 0, \end{aligned} \quad (37)$$

where $R = 1 + g^{tt} g^{xx} E^2 + g^{tt} g^{uu} A_t'^2 + g^{xx} g^{uu} h'^2$ and $f_{\mu\nu} = \partial_{\mu} \delta A_{\nu} - \partial_{\nu} \delta A_{\mu}$ with $\mu, \nu = t, x, y$. The prime denotes the derivative with respect to u -coordinate. Note that $g_{ab}^{-1} = g^{ab}$ and $g_{xx} = g_{yy} = g_{zz}$ in our setup. Then, the quadratic action for the fluctuations can be written as

$$S_{(2)} = \mathcal{N} \int du \mathcal{L}_{(2)}, \quad (38)$$

where

$$\begin{aligned} \mathcal{L}_{(2)} = \frac{1}{2} \frac{(-g)^2}{\mathcal{L}_{(0)}^3} \left[(1 + g^{tt} g^{uu} A_t'^2 + g^{xx} g^{uu} h'^2) g^{tt} g^{xx} f_{tx}^2 + (1 + g^{tt} g^{xx} E^2 + g^{xx} g^{uu} h'^2) g^{tt} g^{uu} \delta A_t'^2 \right. \\ \left. + (1 + g^{tt} g^{xx} E^2 + g^{tt} g^{uu} A_t'^2) g^{xx} g^{uu} \delta A_x'^2 \right. \\ \left. + 2(g^{tt})^2 g^{uu} g^{xx} E A_t' \delta A_t' f_{tx} + 2g^{tt} (g^{xx})^2 g^{uu} E h' \delta A_x' f_{tx} + 2g^{tt} g^{xx} (g^{uu})^2 A_t' h' \delta A_t' \delta A_x' \right] \\ + \frac{1}{2} \frac{(-g)}{\mathcal{L}_{(0)}} \left[(1 + g^{tt} g^{xx} E^2) g^{yy} g^{uu} \delta A_y'^2 + (1 + g^{tt} g^{uu} A_t'^2) g^{xx} g^{yy} f_{xy}^2 + (1 + g^{xx} g^{uu} h'^2) g^{tt} g^{yy} f_{ty}^2 \right. \\ \left. - 2g^{tt} g^{xx} g^{yy} g^{uu} (E A_t' \delta A_y' f_{xy} - E h' \delta A_y' f_{ty} + A_t' h' f_{ty} f_{xy}) \right]. \end{aligned} \quad (39)$$

Here we denote $\mathcal{L}_{(0)}$ as the background Lagrangian density:

$$\mathcal{L}_{(0)} = -\sqrt{-g} R^{1/2}, \quad (40)$$

where $-g = -\det(g_{ab}) = -g_{tt}g_{xx}^3g_{uu}$. We omit the volume element, $\int dt d^3x$, then $S_{(2)}$ precisely denotes the action density. After performing the Fourier transformation, $\delta A_\mu = (2\pi)^{-4} \int d\omega d^3\vec{k} e^{-i\omega t + i\vec{k}\cdot\vec{x}} a_\mu(\omega, \vec{k}, u)$ where $\vec{k}\cdot\vec{x} = k(x\cos\varphi + y\sin\varphi)$ with $k = |\vec{k}|$, we obtain a set of ordinary differential equations for the fields (a_t, a_x, a_y) from the quadratic action above. Introducing gauge-invariant quantities, $\mathcal{E}_L \equiv ka_t \cos\varphi + \omega a_x$ and $\mathcal{E}_T \equiv ka_t \sin\varphi + \omega a_x$, and using the constraint, we can rewrite the equations of motion for \mathcal{E}_L and \mathcal{E}_T . As their explicit forms are not illuminating, we do not write them down here.

To compute the retarded Green's function, we impose the ingoing wave boundary conditions at the horizon [44]. In equilibrium ($E = 0$), the ingoing field at the black hole horizon corresponds to

$$\mathcal{E} = (u - u_H)^{-i\frac{\omega}{4\pi T}} \tilde{\mathcal{E}}, \quad (41)$$

where $\tilde{\mathcal{E}}$ is a regular function at $u = u_H$. Note that in equilibrium \mathcal{E}_L and \mathcal{E}_T are identical since the system is isotropic, therefore we just wrote it as \mathcal{E} . In the steady state, on the other hand, we have the effective horizon outside of the black hole horizon as mentioned in the main text. Then, we consider the Frobenius expansion at $u = u_*$:

$$\mathcal{E}_{L/T} = (u - u_*)^{i\zeta} \bar{\mathcal{E}}_{L/T}, \quad (42)$$

where $\bar{\mathcal{E}}_{L/T}$ is regular at $u = u_*$. Substituting this expression into the equations of motion, we obtain the characteristic equation for ζ . In the case of $\varphi = 0$, for instance, we find two roots:

$$\zeta_0 = 0, \quad \zeta_1 = \frac{2u_*^3 \sqrt{f}(kA'_t + \omega h')}{4f - u_* f'}, \quad (43)$$

where the functions in η_1 are evaluated at the effective horizon $u = u_*$. Here, $\zeta = 0$ corresponds to the ingoing wave boundary condition at the effective horizon [45, 51].

The method for computing the retarded correlators follows Ref. [46]. In addition to the ingoing wave boundary condition, we require to determine the normalization factors at the horizon. Solving the equations of motion with two linearly independent normalization factors, we obtain a set of linearly independent solutions, defining the solution matrix as

$$M(\omega, \vec{k}, u) \equiv \begin{bmatrix} \mathcal{E}_L^{(1)} & \mathcal{E}_L^{(2)} \\ \mathcal{E}_T^{(1)} & \mathcal{E}_T^{(2)} \end{bmatrix}, \quad (44)$$

where $\mathcal{E}_{L/T}^{(i)}$ ($i = 1, 2$) are a set of linearly independent solutions by imposing two normalization factors at the horizon. Using these solutions, the correlator matrix is expressed as

$$\langle J_\mathcal{E}^\alpha J_\mathcal{E}^\beta \rangle(\omega, \vec{k}) = \lim_{u \rightarrow 0} \frac{1}{u} \frac{1}{\omega^2(\omega^2 - k^2)} \left(\begin{bmatrix} \omega^2 - k^2 \sin^2 \varphi & k^2 \sin \varphi \cos \varphi \\ k^2 \sin \varphi \cos \varphi & \omega^2 - k^2 \cos^2 \varphi \end{bmatrix} M'(\omega, \vec{k}, u) M(\omega, \vec{k}, u)^{-1} \right)^{\alpha\beta}, \quad (45)$$

where $J_\mathcal{E}^\alpha$ denotes the dual operator of \mathcal{E}_α with $\alpha = L, T$. We then obtain the aforementioned correlators,

$$\langle J^\mu J^\nu \rangle(\omega, \vec{k}) = \frac{\partial \mathcal{E}_\alpha}{\partial a_\mu} \frac{\partial \mathcal{E}_\beta}{\partial a_\nu} \langle J_\mathcal{E}^\alpha J_\mathcal{E}^\beta \rangle(\omega, \vec{k}). \quad (46)$$

The dispersion relations can be obtained by computing poles in correlators, corresponding to quasi-normal modes in the bulk. To do so, we numerically determine the frequency $\omega(k)$ such that $\lim_{u \rightarrow 0} \det M(\omega, \vec{k}, u) = 0$ is satisfied with a given k and background parameters.

Dispersion relations for general angles

In this Section, we provide additional computations regarding the dispersion relations of the collective excitations and their comparison with the relaxed hydrodynamic theory.

Figure 8 shows the real and imaginary parts of the dispersion relations for several angles with $\tilde{E} = 0.1$ and $\tilde{\rho} = 10^5$ fixed. The black dashed lines correspond to $\text{Re}[\tilde{\omega}] = v_{\text{drift}} \tilde{k} \cos \varphi$ with $v_{\text{drift}} = \alpha \tau \tilde{E}$. The agreement between the theoretical prediction and the numerical data supports the validity of Eq. (6) presented in the main text.

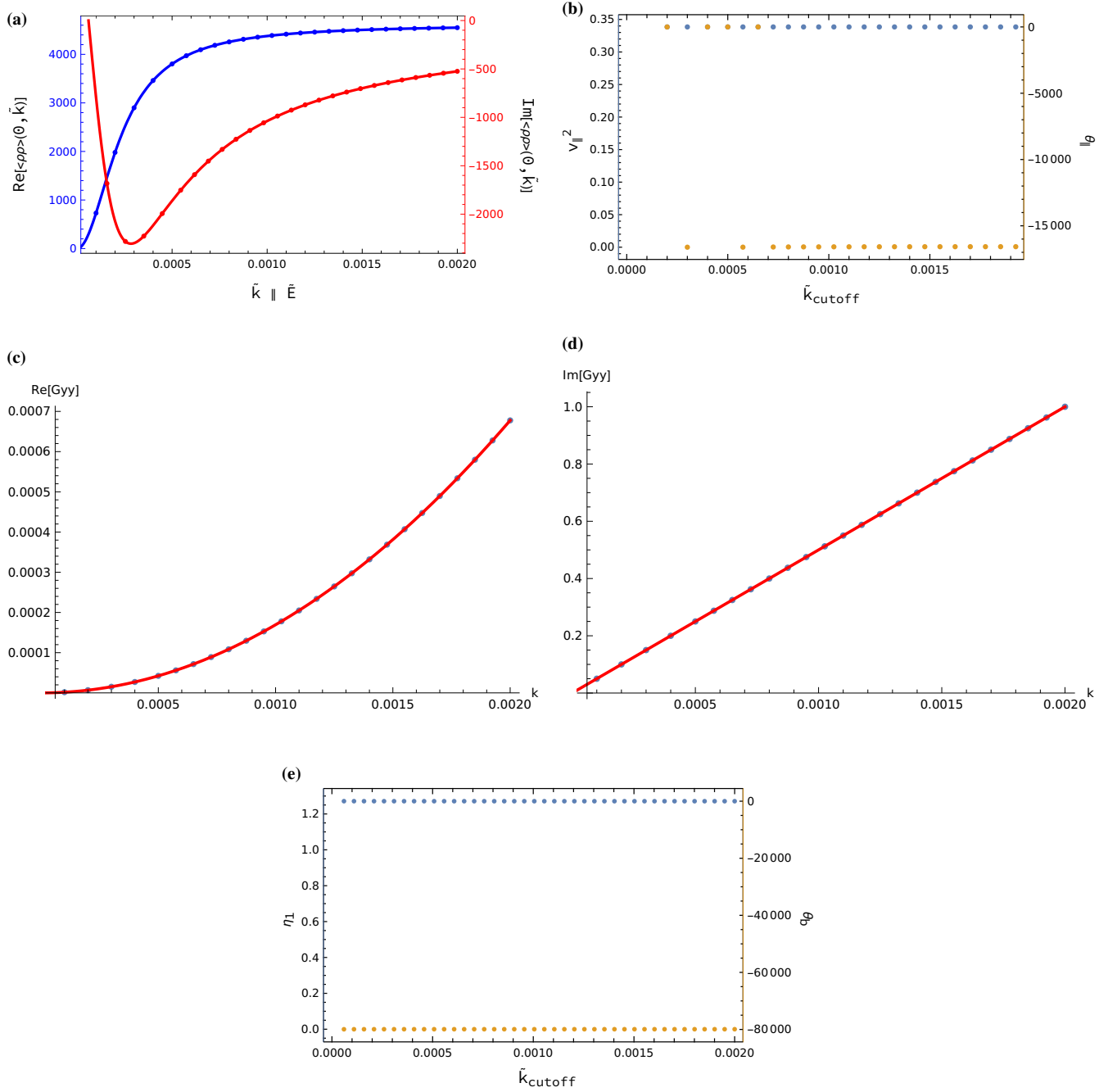


Figure 5. Various plots related to matching parameters between the holographic model and the effective quasihydrodynamic theory. Fig. 5a: a plot of the charge-charge correlator at zero frequency against wavevector for wavevector parallel to the electric field and $E = 5/1000$. The solid lines are fits given by matching our quasihydrodynamic correlator, given in (28), against the data (represented by dots) and extracting v_{\parallel}^2 and θ_{\parallel} from the real part of the Green's function. Fig. 5c and 5d: Plots of the real and imaginary parts of the zero frequency current-current correlator in the y-direction with wavevector transverse to the electric field. The blue dots are numerical data from the holographic model and the red lines represent quadratic (real part) and linear (imaginary part) fits respectively. Fig. 5b: Our data consists of twenty points in the range $\tilde{k} \in [0, 0.002]$. We can check the stability of our fitted coefficients by reducing the largest $\tilde{k} = \tilde{k}_{\text{cutoff}}$ that we include in the data-set that we fit to. We see that v_{\parallel}^2 is stable for all choice of \tilde{k} . Meanwhile, θ_{\parallel} deviates at ultra-low \tilde{k} where the relevant term only makes small contributions to the correlator (c.f. (28)). Fig. 5e: As in Fig. 5b we plot the flow of the fitted coefficient, η_1 , against k_{cutoff} . In this case there are forty-one points. θ_b , also displayed, is given by an analytic expression deriving from (33).

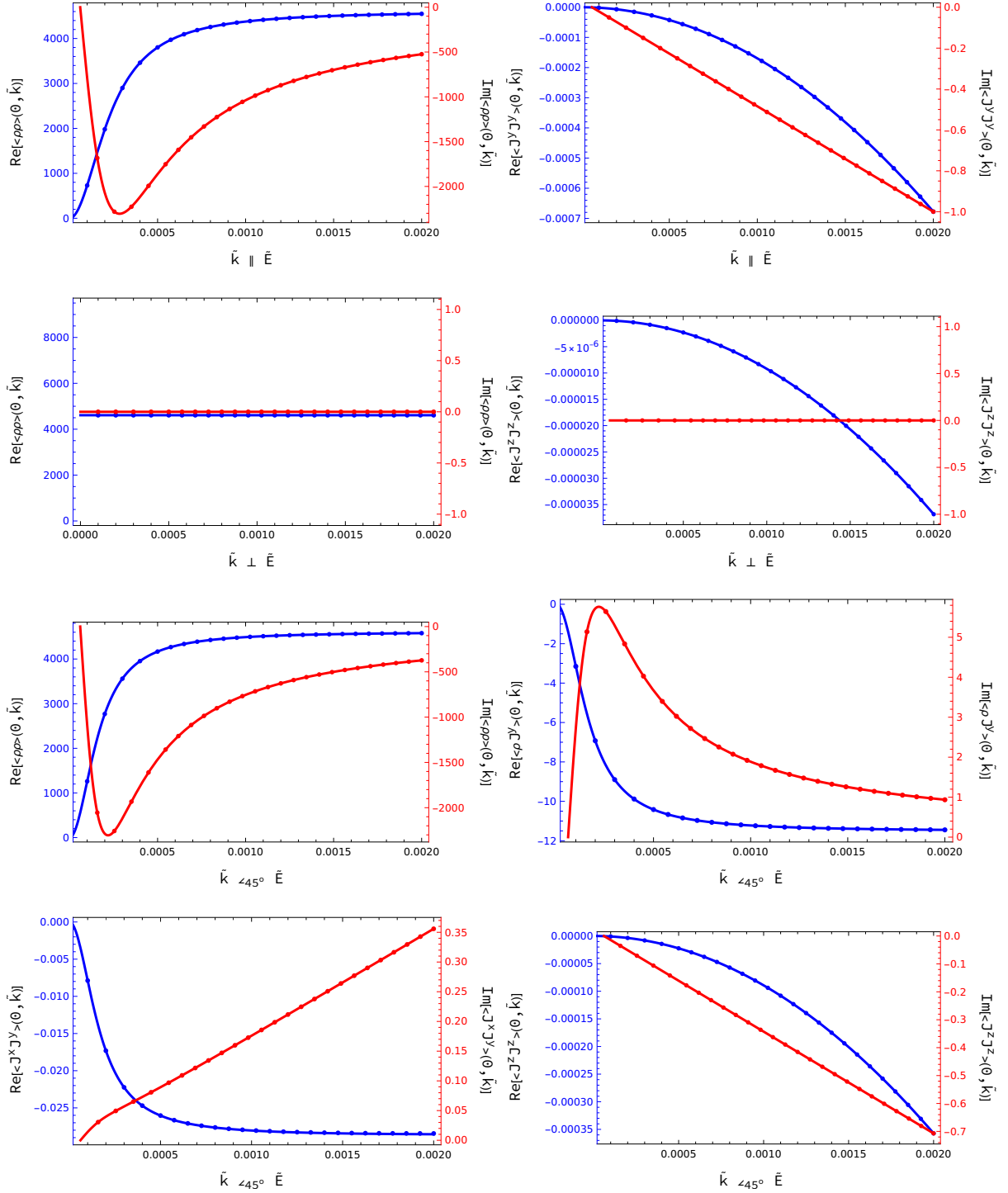


Figure 6. Non-trivial zero frequency correlators against wavevector for various angles at $\tilde{E} = 5/1000$. Solid lines represent the quasihydrodynamic correlators and dots are numerical data.

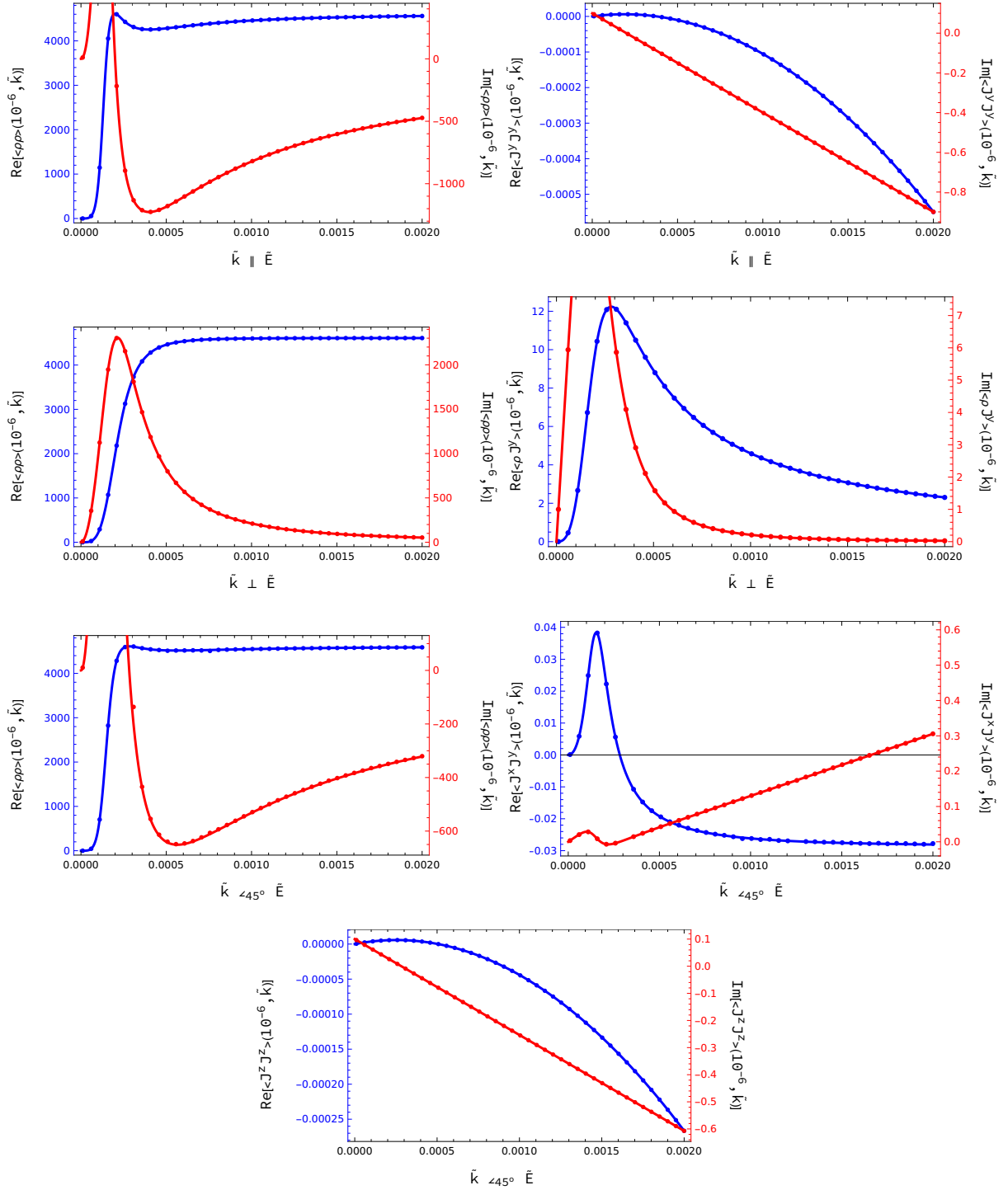


Figure 7. Correlators at $\omega = 10^{-6}$ against wavevector for various angles at $\tilde{E} = 5/1000$. Solid lines represent the quasihydrodynamic correlators and dots are numerical data.

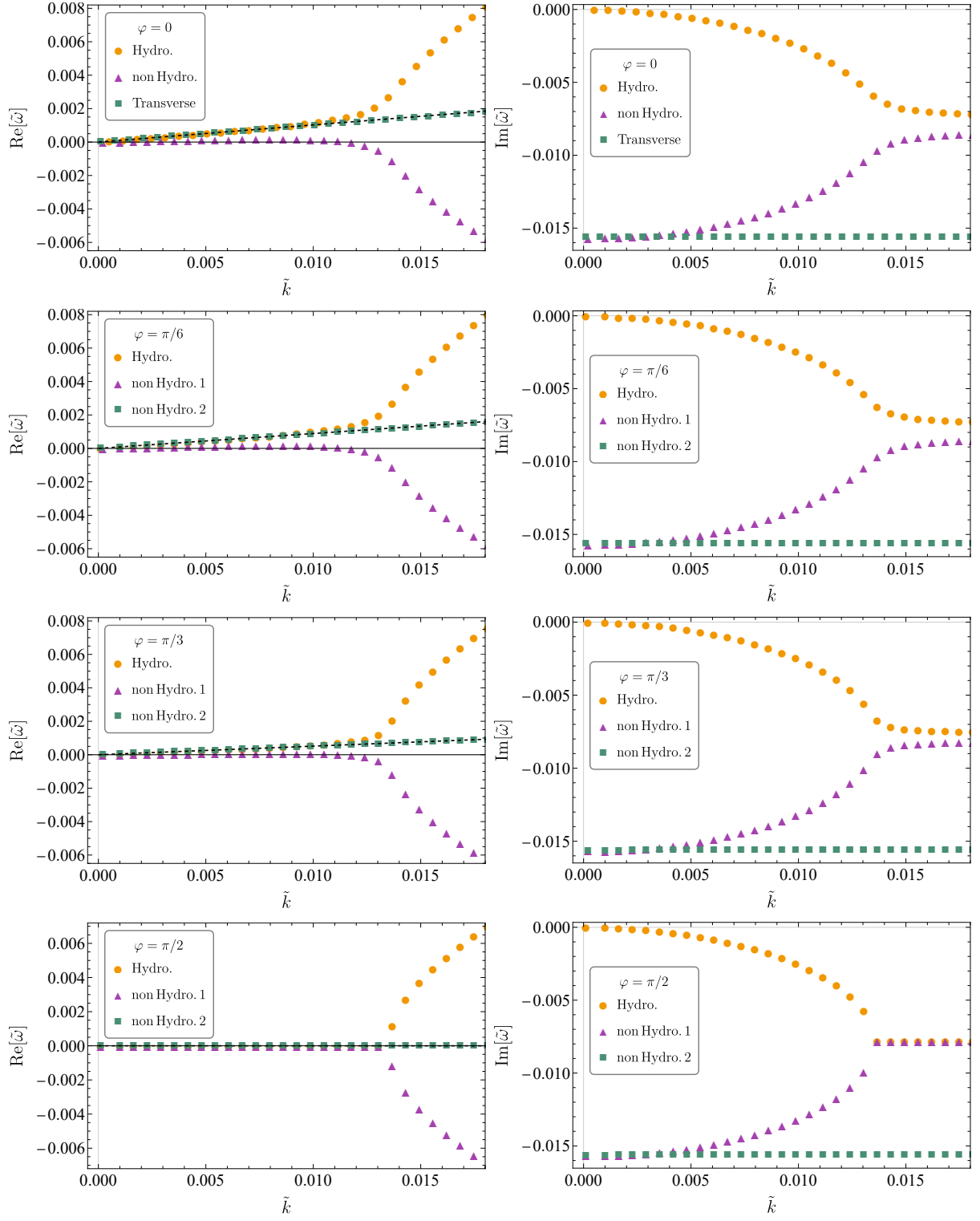


Figure 8. The real (left) and imaginary (right) parts of the dispersion relations for $\varphi = 0, \pi/6, \pi/3, \pi/2$ (from top to bottom) with $\tilde{E} = 0.1$ and $\tilde{\rho} = 10^5$ fixed. The black dashed lines correspond to $\text{Re}[\tilde{\omega}] = v_{\text{drift}} \tilde{k} \cos \varphi$.